Anomalous nano-barrier effects of the ultrathin molybdenum disulfide nanosheets for improving flame retardance of polymer nanocomposites

Journal:	*Journal of Materials Chemistry A*
Manuscript ID:	TA-ART-03-2015-001720.R1
Article Type:	Paper
Date Submitted by the Author:	27-May-2015
Complete List of Authors:	Wang, Dong; University of Science and Technology of China, State Key Lab of Fire Science Song, Lei; University of Science and Technology of China, Zhou, Keqing; University of Science & Technology of China, State Key Lab of Fire Science Yu, Xiaojuan; University of Science and Technology of China, State Key Lab of Fire Science Hu, Yuan; University of Science and Technology of China, State Key Lab of Fire Science Wang, Jian; University of Science and Technology of China, State Key Lab of Fire Science

Anomalous nano-barrier effects of the ultrathin molybdenum disulfide nanosheets for improving flame retardance of polymer nanocomposites

Dong Wang [a], Lei Song [a], Keqing Zhou [a], Xiaojuan Yu [a], Yuan Hu *[a] and Jian Wang*[a]

[a] State Key Laboratory of Fire Science, University of Science and Technology of China, 96 Jinzhai Road, Hefei, Anhui 230026, P. R. China

Corresponding Author

*Tel./Fax: +86-551-63601664. E-mail: yuanhu@ustc.edu.cn. (Yuan Hu)

*Tel./Fax: +86-551-63606463. E-mail: wangj@ustc.edu.cn. (Jian Wang)

Abstract

Polymer/graphene-analogous nanosheets composites had held great promise in improving their physical and mechanical properties in the past few years. Herein, the ultrathin molybdenum disulfide (MoS_2) nanosheets were simultaneously exfoliated and non-covalent modified by ultrasonication in chitosan aqueous solution. Then, the chitosan-modified MoS_2 (CS-MoS_2) nanosheets were transferred from aqueous solution to tetrahydrofuran by a simple solvent exchange method for fabricating epoxy (EP) nanocomposites. Transmission electron microscopy and scanning electron microscopy were performed to display the homogeneous dispersion of CS-MoS_2 in EP matrix. When incorporating 2 wt% CS-MoS_2 into EP matrix, EP nanocomposites exhibited up to 43.3 and 14.6% reduction in peak heat release rate and total heat release derived from cone calorimeter than neat EP, respectively. Moreover, toxic volatiles such as hydrocarbons, aromatic compounds and CO escaped from the flaming EP nanocomposites were decreased compared to that of neat EP, demonstrating the higher smoke safety. Combined with analyses of char residues and thermal stability of EP nanocomposites, the reduced fire hazards of EP nanocomposites could be attributed to the nano-barrier effects of MoS_2, which could effectively inhibit the release of combustible gas to support burning and restrain the effusion of toxic volatiles to cause most of death in fire scene.

1. Introduction

Over the past few years, two-dimensional (2D) materials such as graphene, transition metal dichalcogenides and hexagonal boron nitride have attracted great attention in the field of reinforcing polymer materials[1-3], due to their intrinsic structures and unique material properties[4-7]. For example, graphene-based polymer nanocomposites exhibit superior electrical[8], thermal[9], mechanical[10-13] and flame retardant[14] properties. However, the electrical conductivity of graphene-based polymer nanocomposites restricts their utility in some electrical and electronic applications such as transmission lines, power electronics and capacitors. Thus, it is critical to improve flame retardance while also maintaining the electrical insulation properties and the high dielectric constant of the polymer material to satisfy the aforementioned applications. To our knowledge, epoxy resin (EP) that is a flammable polymer material has been frequently employed in these application[15-17]. As a 2D semiconductor materials, molybdenum disulfide (MoS_2) may be an excellent nanofiller to not impart the electrical conductivity to EP matrix while potentially enhancing its flame retardance at the same time. As we known, MoS_2 has a much lower thermal conductivity than graphene.[18] The low thermal conductivity of MoS_2 is bad for transporting heat in polymer matrix, thus delaying the thermal degradation.[19] Besides, molybdenum-based flame retardants such as molybdenum trioxide, ammonium molybdate have been proved to be excellent smoke suppressants.[20,21]

Like other 2D materials, the dispersion level of MoS_2 nanosheets in polymer matrix and the interfacial interaction between MoS_2 and polymer matrix should be settled to achieve optimal reinforcement in the properties of MoS_2/polymer composite.[22,23] Generally, the processing method of graphene-based polymer composite and exfoliation degree of bulk graphite play the key roles in the dispersion state of graphene nanosheets in polymer matrix.[24,25] The solution blending has been proved to fabricate the well-dispersed graphene-based polymer nanocomposites,[26] likewise applied to the processing of MoS_2/EP nanocomposite. Because of strong intralayer covalent bonding and weak interlayer van deer Waals interaction of bulk MoS_2[27] the ultrathin MoS_2 nanosheets have been prepared by mechanical exfoliation[28], liquid exfoliation[29], ion intercalation technique[30] and chemical vapor deposition growth[31]. In particular, the liquid sonication accompanied by nature polymeric surfactant can stabilize exfoliated MoS_2 nanosheets against re-aggregation and provide the hydrogen-bond interaction possibility between MoS_2 nanosheets and polar polymer matrix.[32]

Chitosan (CS), an natural polymer cationic surfactants with multi-hydroxyl groups and multi-amino groups, has been reported to act as an excellent stabilizer for dispersing multi-walled carbon nanotubes in aqueous solution.[33] Chitosan modified MoS_2 (CS-MoS_2) nanosheets could be homogeneously dispersed in water because the attached chitosan donates partial positive charge to CS-MoS_2 system,[34] which provides electrostatic repulsion force against the van der Waals force of the sheets. To prepare CS-MoS_2/EP nanocomposites by the solvent blending method, CS-MoS_2 nanosheets should be dispersed into the tetrahydrofuran firstly. Nevertheless, CS-MoS_2 nanosheets tend to stacking during drying process and the van der Waals attractive interactions between the sheets prevent the re-entry of solvent molecules into interlayer spaces of CS-MoS_2.[35] Thus, we proposed that CS-MoS_2 aqueous dispersion is firstly centrifuged, and then the wet CS-MoS_2 sediment is re-dispersed in organic solvents such as tetrahydrofuran. After several repeated cycles of centrifugation and washing with organic solvents, CS-MoS_2 is homogeneously transferred into organic solvents. Moreover, the hydroxyl and amino group onto MoS_2 nanosheet derived from chitosan will form the strong hydrogen-bond and chemical bond interaction with EP matrix.[36]

To our knowledge, the flame retardant properties and mechanism of polymer materials reinforced by MoS_2 nanosheets have yet to be investigated in depth. Herein, it was proposed that the bulk MoS_2 were exfoliated and non-covalently functionalized in CS aqueous solution by the sonication method. Then the wet CS-MoS_2 was homogeneously dispersed in tetrahydrofuran by a simple solvent exchange method and used to prepare CS-MoS_2/EP nanocomposite. This study highlights the anomalous nano-barrier effects of the well-dispersed CS-MoS_2 nanosheets which could significantly reduce fire hazards of EP nanocomposites.

2. Experimental

2.1 Exfoliation of MoS_2 assisted with chitosan solution

The ultrathin MoS_2 nanosheets obtained via the polymer-assisted exfoliation process was shown in Scheme 1. Bulk MoS_2 powder was dispersed in a certain amount of chitosan solution (0.5 wt% chitosan was dissolved in acetic acid aqueous solution).

The mixture was carried out in the sonication ice-bath for 36 h and then centrifuged at 3000 rpm for 15 min to separate the stale MoS_2 suspension (Fig. S1) from the non-exfoliated MoS_2 sediments. The MoS_2 suspension was placed for two weeks and subsequently centrifuged at 8000 rpm for 20 min to get the wet MoS_2 sediments after washing with distilled water several times. A part of the wet MoS_2 sediments was dried at 60 °C overnight for the characterization. The other part was weighed to confirm its solid content for the fabrication of CS-MoS_2/EP nanocomposites.

2.2 Fabrication of CS-MoS_2/EP nanocomposites

CS-MoS_2/EP nanocomposites were prepared by the solvent blending method, keeping the nanofiller loading at 0.5 wt%, 1 wt% and 2 wt% respectively. Firstly, the tetrahydrofuran dispersion of CS-MoS_2 nanosheets was prepared by the simple solvent exchange method. The calculated wet CS-MoS_2 sediments were re-dispersed in tetrahydrofuran and then re-centrifuged at 8000 rpm for 10 min. After several repeated cycles of centrifugation and washing with tetrahydrofuran, the ultrathin CS-MoS_2 nanosheets is homogeneously dispersed into tetrahydrofuran. Afterwards, neat EP was added into the above dispersion and stirred with ultrasonic agitation for 6 h. The homogeneous mixture was heat at 80 °C to remove tetrahydrofuran and then the melt 4,4$'$-aminodiphenylmethane was added with stirring for several minutes. Finally, the above mixture was poured in 100×100×3 mm^3 teflon mold, cured at 100 °C for 2 h and post cured at 150 °C for 2 h. For comparison, the wet CS-MoS_2 sediments were replaced by bulk MoS_2 to fabricate MoS_2/EP nanocomposites.

2.3 Characterization

Transmission electron microscopy (TEM) (JEM-2100F, Japan Electron Optics Laboratory Co., Ltd.) was used to investigate the morphology of exfoliated MoS_2 nanosheet and the ultrathin section of EP nanocomposites. The accelerating voltage was 200 kV. Atomic force microscopy (AFM) observation was performed on the DI Multimode V in tapping-mode. Fourier transform infrared (FT-IR) spectra analyses were operated on samples pressed into tablets with KBr powder in the range of 4000-400 cm^{-1} using a Nicolet 6700 spectrometer (Nicolet Instrument Corporation, US). UV-vis absorption measurements were taken using a UV-visible spectrophotometer (Cary 100 Bio, Varian, America). Laser Raman spectroscopy measurements were performed using a SPEX-1403 laser Raman spectrometer (SPEX Co., USA) with excitation provided in back-scattering geometry by a 514.5 nm argon laser line. Thermogravimetric analysis (TGA) was carried out using a Q5000 thermoanalyzer instrument (TA Instruments Inc., New Castle, DE) under an air flow of 20 $mL\cdot min^{-1}$. The temperature was increased from room temperature to 700 °C at a linear heating rate of 20 $°C\cdot min^{-1}$. Microstructures of the fracture surface and char residues were observed by a PHILIPS XL30E scanning electron microscope (SEM). Differential scanning calorimeter (DSC) was performed using a Q2000 DSC instrument (TA Instruments Inc.). Samples (2-4 mg) were heated from 30 to 200 °C at a linear heating rate of 10 $°C\cdot min^{-1}$; The temperature was kept at 200 °C for 10 min and then decreased from 200 to 0 °C at a linear rate of 10 $°C\cdot min^{-1}$. The heating-cooling cycle was performed through the 1st cooling cycle after erasing the thermal history. Microscale combustion colorimeter (MCC, Govmark Organization, Inc., Farmingdale, NY) was used to investigate the flammability of EP nanocomposites based on ASTM D7309-07. Samples of about 5 mg were heated in N_2 atmosphere at a constant heating rate of 1 °C·s^{-1} from room temperature to 650 °C. The decomposition products were mixed with oxygen (20 mL·min^{-1}) and then combusted in the combustion furnace at 900 °C. Fire hazards of samples were performed on a cone calorimeter (Fire Testing Technology, U.K.) according to ASTM E1354/ISO 5660. Each sample (100 × 100 × 3 mm^3) was wrapped in an tinfoil and exposed horizontally to a 35 kW/m^2 external heat flux. The thermogravimetric analysis/infrared spectrometry (TG-IR) was performed using the TGA Q5000 IR thermogravimetric analyzer coupled with the Nicolet 6700 FT-IR spectrophotometer.

3. Results and discussion

3.1 Characterization of CS-MoS_2 nanosheets

The morphology of MoS_2 nanosheets before and after chitosan-assisted sonication treatment were investigated by TEM. Fig. 1a shows the TEM image of bulk MoS_2, from which the large-area stacked nanosheets with length up to 1 μm and width of about 500 nm are clearly visible. After exposure to sonication, the seriously stacked layers of bulk MoS_2 are exfoliated to few and mono-layered structures. Compared to bulk MoS_2, CS-MoS_2 exhibits a thinner and smaller nanoplatelet shape. Tapping-mode AFM is further used to determine size and thickness of 2D CS-MoS_2 nanosheets with atomic thickness. The CS-MoS_2 nanosheets without the free CS were prepared from the supernatant via repeating the washing and centrifugation steps more than ten times, and then re-dispersed in water. The AFM samples were prepared by casting a few drops of the above dispersions on Si/SiO_2 substrate. As shown in Fig. 2c, the exfoliated CS-MoS_2 nanosheets are tens or hundreds nanometers wide, with the thickness varied from 0.8 to 1.3 nm, which is fairly consistent with single-layer MoS_2 after exfoliation.[37,38]

The successful exfoliation of MoS_2 in the aid of CS was further confirmed by Raman spectrum and UV/Vis. Two characteristic vibration modes E^1_{2g} (in-plane) and A_{1g} (out-of-plane) of bulk MoS_2 are located at 380.1 and 407.9 cm^{-1}. For CS-MoS_2, E^1_{2g} peak shifts to a higher frequency and A_{1g} peaks of MoS_2 transfers to a lower frequency, indicating that CS-MoS_2 are thinner than bulk MoS_2.[39] The peak frequency difference can be used to estimate the numbers of MoS_2 monolayer and the value of 23.8 cm^{-1} for as-obtained CS-MoS_2 implies an average thickness of about 5 monolayers.[27] In addition, Raman bands of CS-MoS_2 with full-width at half maximum of 11.9 cm^{-1} for E^1_{2g} and 12.1cm^{-1} for A_{1g} are broader than the bulk MoS_2 with full-width at half maximum of 5.4 cm^{-1} for E^1_{2g} and 5.5 cm^{-1} for A_{1g}, attributed to the phonon confinement of nano-sized layer structure.[40] The absorption spectrum of the ultrathin CS-MoS_2 dispersion shows the two characteristic absorption peaks at 615 and 675 nm, arisen from direct transition from the valance band to the conduction band at the K-point of the Brillouin zone, known as the B and A transitions,[41] respectively. The value of excitons exhibits a blue shift compared with the data for the bulk MoS_2 (748 nm) in a previous reports, due to the quantum-size confinement.[42,43]

To investigate the non-functionalization of MoS_2 nanosheets by CS, CS-MoS_2

was characterized by FT-IR and TGA. Fig. 3a displays the FT-IR spectra of the bulk MoS_2, CS and CS-MoS_2. In the spectrum of MoS_2, the water bonding at 1634 cm^{-1} and the broad stretching band of –OH centered at 3430 cm^{-1} can be observed. As for the pure CS, there are the two characteristic peaks at 1661 and 1598 cm^{-1} assigned to C=O stretching band of the amide groups and N−H bending of secondary amide, respectively.[44] As been observed in the spectrum of CS-MoS_2, the characteristic peaks of the amide groups disappears, and two new peaks at 1719 and 1624 cm^{-1} assigned to C=O stretching band of carboxyl groups and N−H bending of primary amide emerge, probably because the amide groups of CS hydrolyzed in the preparation of CS-MoS_2. The other peaks of CS-MoS_2 is similar to those of CS, demonstrating that chitosan molecules were stabilized onto MoS_2 nanosheets. Thermal decomposition curves of bulk MoS_2, CS and CS- MoS_2 in air atmosphere are shown in Fig. 3b. Bulk MoS_2 reveals an obvious mass loss between 500 and 600 °C, corresponding to the oxidation process of MoS_2 to MoO_3.[45] The TGA profile of CS-MoS_2 is similar to that of CS, exhibiting a successive decrease from 200 to 600 °C. Based on the amount of their char residues in 700 °C, the proportion of chitosan in CS-MoS_2 is calculated to be 13.5%, suggesting the high degree of surface modification.

3.2 Dispersion

To learn about the dispersion level of bulk MoS_2 and CS-MoS_2 in epoxy resin, the freeze-fractured surface microstructures of EP nanocomposites were investigated by SEM. According to the previous works, the facture roughness of polymer nanocomposites reflects the dispersion level and interfacial interaction to some degree.[46,47] As could be observed in Fig. 4a, neat EP displays a smooth fracture surface. It is clear that the fracture surface roughness of CS-MoS_2/EP nanocomposites get increased with the increased addition of CS-MoS_2. Meanwhile, the fracture surface of 2 wt% CS-MoS_2/EP are much rougher than that of 2 wt% MoS_2/EP, indicating the better dispersion and stronger interfacial interaction of 2 wt% CS-MoS_2/EP nanocomposites. In addition, it is observed that numerous MoS_2 agglomerates are pulled out of MoS_2/EP nanocomposite. Nevertheless, few MoS_2 agglomerates emerge in the SEM images of CS-MoS_2/EP nanocomposites, because most of the ultrathin CS-MoS_2 nanosheets are uniformly embedded into EP matrix.

To further evaluate the dispersion level of bulk MoS_2 and CS-MoS_2 in epoxy matrix, their inner structures are directly observed by TEM. As shown in Fig. 5a, a large number of bulk MoS_2 nanosheets are agglomerated together in 2 wt% MoS_2/EP nanocomposites. In contrast, Fig. 5b shows the ultrathin CS-MoS_2 nanosheets are well dispersed in the matrix with the intercalated and exfoliated structure. In short, CS-MoS_2 nanosheets exhibit the better dispersion in EP matrix and compatibility with the matrix than bulk MoS_2, because of the thinner structure and stronger interfacial interaction.

3.3 Thermal behavior

Based on the fact that thermal behavior of burning polymer closely relates to flame retardance, DSC and TGA are usually applied to investigate thermal behavior of polymer material.[48] After erasing the thermal history, the DSC profiles of pure EP and its nanocomposites are recorded through the second heating scan. Fig. S2 shows the T_g of neat EP is clearly observed at 130.6 °C. The T_gs of CS-MoS_2/EP and MoS_2/EP nanocomposites gradually increase when the contents of CS-MoS_2 and bulk MoS_2 increase, respectively. It is observed that 2 wt% bulk MoS_2 results in the T_g slightly increased to 133.4 °C, but the same loading of CS-MoS_2 leads to the T_g significantly increased by 10.3 °C. The obvious T_g increase of CS-MoS_2/EP nanocomposites originates from the restriction of polymer segmental mobility, due to the large contact area of the 2D geometry and strong non-covalent/covalent polymer-nanofiller interactions.

TG and DTG curves of neat EP and its nanocomposites are plotted in Fig. 6. Based on TG profiles, neat EP and EP nanocomposites have two stages of thermal decomposition process, corresponding to the degradation of molecular chain and oxidation of char residue. The temperatures of the maximum mass loss rate of molecular chain and the maximum char oxidation rate are called $T_{\max1}$ and $T_{\max2}$ for short, respectively. As can be observed, all the $T_{\max1}$s are below 400 °C, indicating the survival of MoS_2 during polymer degradation. Nevertheless, all the $T_{\max2}$s clearly exceed 500 °C, implying the oxidation of MoS_2 to molybdenum oxide during char oxidation. Meanwhile, it is found that the maximum mass loss rates of EP nanocomposites are much lower than neat EP, but the maximum char oxidation rates of EP nanocomposites are versa, probably because the large contact area of 2D MoS_2 inhibits the release of pyrolysis products during the degradation of molecular chain and restrained pyrolysis products lose the shield of 2D MoS_2 to escape during char oxidation.

3.4 Flame retardance

MCC is an effective bench-scale measurement system for evaluating the combustion properties of materials and only needs milligram quantities of the specimen.[49] The HRR curves of neat EP and its nanocomposites derived from MCC are plotted in Fig. 7. The PHRR value has been often regarded as the most index of the flame retardance. Compared to neat EP, the PHRR values of CS-MoS_2/EP nanocomposites are decreased by 12.0%, 28.5% and 33.3% with the loading of CS-MoS_2 increasing, respectively. Moreover, 2 wt% bulk MoS_2 powders only gives rise to a 20.7% reduction in PHRR, indicating the more superior flame retardant efficiency of CS-MoS_2.

To further investigate the flame retardance of EP nanocomposites under real condition, the HRR profiles originated from cone calorimeter are plotted in Fig. 8 and the related data are recorded in Table 1. Cone calorimeter works based on the oxygen consumption principle that the heat release of burning materials is proportional to the oxygen consumption.[50] The PHRR of neat EP reaches up to 1592 kW/m^2, declaring the high inflammability. When incorporating CS-MoS_2 into the EP matrix, the PHRR values of EP nanocomposites are gradually decreased with the content gradually increasing. 2 wt% CS-MoS_2 makes the PHRR of EP nanocomposite significantly reduced to 902 kW/m^2, corresponding to 43.3% reduction compared to neat EP. On the contrary, the PHRR of 2 wt% MoS_2/EP nanocomposite is only decreased by 26.0%. THR is the sum of the HRR of materials during the whole burning process.

The THR values of CS-MoS_2/EP nanocomposites decrease progressively until the additive amount is increased to 1 wt%. The decreased THR could be explained by the large contact area of CS-MoS_2 nanosheets to suppress the release of combustible gas and then promote charring, which is further evidenced by the digital images (Fig. S3) of char residues after the cone test. When CS-MoS_2 amount further add up to 2 wt%, the THR value is increased to 33.9 MJ/m^2 yet, probably because the stronger suppression of more CS-MoS_2 nanosheets farther reduces the effusion rate of combustible gas, causing the more complete oxidative combustion of the combustible volatiles such as hydrocarbons to produce more heat. In the case of MoS_2/EP, the PHRR value is higher than that of neat EP instead, which will be discussed behind.

When the combustible gas of the material exposed to thermal radiation reaches the critical concentration, it is ignited. From Table 1, it is found that TTIs of EP nanocomposites are slightly prolonged compared to pure EP, probably attributed to the 2D structure of MoS_2 nanosheets to suppress the release of combustible gas at ignition stage.

FGI, defined as the ratio of PHRR and time to PHRR, is an overall index to evaluate the flame retardance of materials. As is well-known, the lower FGI value means the higher flame retardance. The FGI value of neat EP is 17.3 kW/ ($m^2 \cdot s$), but those of 0.5 wt%, 1 wt%, 2 wt% CS-MoS_2/EP and MoS_2/EP nanocomposites are 12.4, 12.2, 8.4 and 11.8 kW/($m^2 \cdot s$), respectively.

3.5 Smoke toxicity

It is well-known that toxic pyrolysis products escape from burning materials, being more harmful than thermal hazards. In order to study pyrolysis toxicity to human, TG-IR is usually utilized to half-qualitatively identify pyrolysis components by the location of their infrared characteristic peaks and half-quantitatively compare pyrolysis concentration by the intensity of their infrared characteristic peaks. Fig. 9a shows total gas volatile intensity *versus* time curves of neat EP, 2 wt% CS-MoS_2/EP and MoS_2/EP nanocomposites. It is clearly observed that the CS-MoS_2/EP nanocomposite releases the lowest pyrolysis products, indicating the lowest smoke toxicity. Moreover, almost the same peaks of neat EP, 2 wt% CS-MoS_2/EP and MoS_2/EP nanocomposites emerge in the FT-IR spectra of pyrolysis products at the T_{max} (defined as the temperature of the maximum release rate) in Fig. S3, further suggesting that the existence of CS-MoS_2 and bulk MoS_2 don't change pyrolysis way of epoxy molecules. From the FT-IR spectra, it can be found that hydrocarbons (3100-2800 cm^{-1}), CO (2180 cm^{-1}) and aromatic compounds (1605, 1510 and 1460 cm^{-1}) are escaped, tremendously threatening human trapped in fire. Hydrocarbons tend to aggregate into smoke particles for reducing visibility and act as “fuel” to support burning. Similarly, aromatic compounds are also inclined to aggregate into smoke particles and are harmful to human health. In the case of toxicity, CO is more poisonous than hydrocarbons and aromatic compounds, causing most of the dead in fire. As can be observed in Fig. 9, hydrocarbons, aromatic compounds and CO released from EP nanocomposites are decreased compared to neat EP, demonstrating the lower smoke toxicity of 2 wt% CS-MoS_2/EP and MoS_2/EP nanocomposites, which could win more time for fire rescue.

3.6 Analysis of char residues

To further figure out the flame-retardant mechanism of the condensed phase and/or gas phase, the investigation of char residues after the cone test contributes to understand how MoS_2 nanosheets act in burning EP.[51] Digital photos of char residues in tinfoil boxes (Fig. S4) reveal that a few and loose char residues scatter in EP box, but plentiful and compact char residues neatly disperse in the CS-MoS_2/EP boxes. For 2wt% CS-MoS_2/EP nanocomposites, the char residues completely cover the whole box except a few holes. As to 2wt% MoS_2/EP nanocomposites, there are less char residues irregularly distributed in the box, by comparison. The part char residues appearance of EP nanocomposites get purple especially 2wt% MoS_2/EP, due to the oxidation of MoS_2 to molybdenum oxide.

Furthermore, the microstructures of external and internal char residues were studied by SEM. Fig. 10a and b are SEM images of the microstructures of external and internal char residues, respectively. Compared to neat EP and 2wt% MoS_2/EP, no holes emerge in the external char of 2wt% CS-MoS_2/EP in the SEM image at low magnification. The SEM image of external char of neat EP at high magnification shows the smooth appearance. Unlike neat EP, numerous granular molybdenum oxide forms onto external char residues of EP nanocomposites. SEM images of internal char residues also demonstrate that internal char layers of CS-MoS_2/EP are more compact than that of MoS_2/EP. It is clearly observed that many flake-like MoS_2 still exist in internal char residues of EP nanocomposites, probably because of oxygen deprivation in underlying polymer during burning. To confirm the survival of MoS_2 nanosheets, internal char residues are investigated by Raman spectroscopy (Fig. 11). In the Raman spectra of EP nanocomposites, the characteristic bands at 383 and 408 cm^{-1} are assigned to MoS_2. Obviously, the intensities of the two characteristic bands of CS-MoS_2/EP are much stronger than that of MoS_2/EP, indicating more MoS_2 survived in internal char residues of CS-MoS_2/EP. Except the two MoS_2 bands, D band at 1350 cm^{-1} and G band at 1602 cm^{-1} emerge in Raman spectra.[19,50] According to previous works, the compactness of char residues closely relates to the degree of graphitization of char and the degree of graphitization is evaluated by the ratio of integrated intensities of D and G bands (I_D/I_G).[51] The lower the ratio of I_D/I_G means the higher graphitization degree of the char. The internal char residues of CS-MoS_2/EP nanocomposites displays the lowest I_D/I_G, suggesting the formation of the densest char.

3.7 Flame retardant mechanism

Kim *et al.*[30] have demonstrated that MoS_2 nanosheets are anomalously included in polymer matrix. Herein, based on the dispersion analysis, it is assumed that unidirectional CS-MoS_2 or bulk MoS_2 nanosheets are homogeneously and poorly distributed in EP matrix respectively, as shown in Fig. 12. The thermal analyses of MoS_2 and EP nanocomposites show clearly that T_{max} of MoS_2 obviously exceed that of EP nanocomposites, meaning the high thermal-oxidative resistance of MoS_2 during burning. Besides, based on the analyses of smoke toxicity and char residues, MoS_2 nanosheets mainly act in the condensed phase. Combined with the analysis of flame retardance, it is reasonably speculated that independent MoS_2 nanosheets in the EP matrix act as nano-barriers to restrain the permeation of heat and oxygen, and inhibit the effusion of toxic volatiles.[52,53] In order to profoundly understand the nano-barrier effects of MoS_2 nanosheets, it is vividly illustrated how the MoS_2 nanosheets work in the flaming CS-MoS_2/EP nanocomposites in Scheme 2. As shown, the flame spreads onto the surface of burning polymer and then propagates inwards. Simultaneously, external heat mixed with oxygen permeate into underlying materials to trigger internal pyrolysis. Moreover, the heat radiation and oxygen concentration to permeate gradually drop with the depth of permeation increasing. Inside CS-EP nanocomposites, each independent CS-MoS_2 nanosheet serves as a nano-barrier to prevent the permeation of external heat as well as oxygen, and retard the escape of pyrolysis products such as hydrocarbons, CO and aromatic compounds. Nano-barrier effects of CS-MoS_2 nanosheets result in "tortuous path" to lower the release rate of combustible gas including hydrocarbons to support combustion, thus decreasing the heat release rate. Furthermore, nano-barrier effects of CS-MoS_2 nanosheets also promote the aggregation of hydrocarbons and aromatic compounds to produce smoke particles and then accumulate into char residues, thus reducing the total heat release. Unfortunately, the low release rate of combustible gas may facilitate its complete oxidation-combustion to produce more THR.

Therefore, the flame retardance of EP nanocomposites with the different content of CS-MoS_2 are attributed to the quantities of nano-barriers in polymer matrix. Obviously, the quantities of nano-barriers get increased with the addition of CS-MoS_2 nanosheets increasing, so the suppression on the release rate of combustible gas becomes strengthened, gradually decreasing PHRR values of CS-MoS_2/EP nanocomposites. It is noteworthy that the growing CS-MoS_2 nanosheets would improve the nano-barrier effects to promote charring and oxidation-combustion. Analyzing the THR results of CS-MoS_2/EP nanocomposites, it could be concluded that the nano-barrier effects to promote charring dominate in reducing THR and the nano-barrier effects to promote oxidation-combustion grow faster with the increasing CS-MoS_2 nanosheets than the former. Because of the bad exfoliation of bulk MoS_2 and poor dispersion, the quantities and efficiency of nano-barriers of bulk MoS_2 nanosheets are much less than CS-MoS_2 nanosheets, interpreting the worse flame retardance of MoS_2/EP compared to that of CS-MoS_2/EP. For MoS_2/EP nanocomposites, the THR is slightly higher than that of neat EP, probably ascribed to two aspects: for one thing, the nano-barrier effects to promote oxidation-combustion slightly surpass that to promote charring; for another thing, the poor-dispersed bulk MoS_2 nanosheets tend to oxidize, generating heat.

4. Conclusion

In this work, bulk MoS_2 nanosheets were exfoliated and non-covalently modified to obtain the ultrathin CS-MoS_2 nanosheets by ultrasonication in chitosan aqueous solution. Then the wet CS-MoS_2 sediment were dispersed in tetrahydrofuran via the solvent exchange method and used to fabricate EP nanocomposites by the solution-based process. Due to the ultrathin structure and polymeric modification of MoS_2 nanosheets, the CS-MoS_2 nanosheets were well dispersed in EP matrix, confirmed by SEM and TEM results. DSC and TGA reveal that the nano-barrier effects of MoS_2 nanosheets restrict the motion of EP molecules and the effusion of pyrolysis products. Importantly, the nano-barrier effects of MoS_2 nanosheets could restrain the permeation of external heat as well as oxygen, and inhibit the escape of toxic volatiles, significantly improving the flame retardance of EP nanocomposites and reducing the smoke toxicity. The flame-retardant mechanism of condensed phase of EP nanocomposites were demonstrated by TG-IR and char residues analyses, also verifying the nano-barrier effects of MoS_2 nanosheets. This work will provide theoretical basis of flame retardance to MoS_2- based polymer nanocomposites.

Acknowledgements

The work was financially supported by the National Natural Science Foundation of China (NO. 21374111) and National Natural Science Foundation of China (51303165).

References and notes

(1) Yuan, B. H.; Bao, C. L.; Qian, X. D.; Song, L.; Tai, Q. L.; Liewc, K. M.; Hu, Y. Design of artificial nacre-like hybrid films as shielding to mitigate electromagnetic pollution. *Carbon.* **2014***, 75*, 178-189.

(2) Eksik, O.; Gao, J.; Shojaee, S. A.; Thomas, A.; Chow, P.; Bartolucci, S. F.; Lucca, D. A.; Koratkar. N. Epoxy nanocomposites with two-dimensional transition metal dichalcogenide additives. *ACS Nano.* **2014**, *8*, 5282-5289.

(3) Song, W. L.; Wang, P.; Cao, L.; Anderson, A.; Meziani, M. J.; Farr, A. J.; Sun. Y. P. Polymer/Boron nitride nanocomposite materials for superior thermal transport performance. *Angew. Chem., Int. Ed.* **2012***, 51,* 6498-6501.

(4) Novoselov, K. S.; Geim, A. K.; Morozov, S. V.; Jiang, D.; Katsnelson, M. I.; Grigorieva, I. V.; Dubonos. S. V.; Firsov, A. A. Two-dimensional gas of massless Dirac fermions in graphene. *Nature.* **2005***,* 438, 197-200.

(5) Zhang, Y. B.; Tan, Y. W.; Stormer, H. L.; Kim, P. Experimental observation of the quantum Hall effect and Berry's phase in graphene. *Nature.* **2005***, 438,* 201-204.

(6) Splendiani, A.; Sun, L.; Zhang, Y. B.; Li, T. S.; Kim, J.; Chim, C. Y.; Galli, G.; Wang, F. Emerging photoluminescence in monolayer MoS2. *Nano Lett.* **2010***, 10,* 1271-1275.

(7) Watanabe, K.; Taniguchi, T.; Kanda, H. Direct-bandgap properties and evidence for ultraviolet lasing of hexagonal boron nitride single crystal. *Nat. Mater. 3,* 404-409.

(8) Stankovich, S.; Dikin, D. A.; Dommett, G. H. B.; Kohlhaas, K. M.; Zimney, E. J.; Stach, E. A.; Piner, R. D.; Nguyen, S. T.; Ruoff, R. S. Graphene-based composite materials. *Nature.* **2006***, 442,* 282-286.

(9) Liang, J. J.; Huang, Y.; Zhang, L.; Wang, Y.; Ma, Y. F.; Guo, T. Y.; Chen, Y. S. Molecular-Level Dispersion of graphene into Poly(vinyl alcohol) and effective reinforcement of their nanocomposites. *Adv. Funct. Mater.* **2009***, 19,* 2297-2302.

(10) Rafiee, M. A.; Rafiee, J.; Wang, Z.; Song, H. H.; Yu, Z. Z.; Koratkar, N. Enhanced mechanical properties of nanocomposites at low graphene content. *ACS Nano*. **2009***, 3,* 3884-3890.

(11) Wang, X. B.; Weng Q. H.; Wang, X.; Biomass-directed synthesis of 20 g high-quality boron nitride nanosheets for thermoconductive polymeric composites. *ACS Nano*. **2014**, *8*, 9081-9088.

(12) Hsiao, M. C.; Liao, S. H.; Lin, Y. F.; Wang, C. A.; Pu, N. W.; Tsai, H. M.; Ma, C. C. M. Preparation and characterization of polypropylene-graft-thermally reduced graphite oxide with an improved compatibility with polypropylene-based nanocomposite. *Nanoscale*. **2011**, *3*, 1516-1522.

(13) Wang, X. B.; Zhi, C. Y.; Li, L.; “Chemical blowing” of thin-walled bubbles: high-throughput fabrication of large-area, few-layered BN and Cx-BN nanosheets. *Adv. Mater.* **2011**, *23*, 4072-4076.

(14) Wang, D.; Zhang, Q. J.; Zhou, K. Q.; Yang, W.; Hu, Y.; Gong, X. L. The influence of manganese-cobalt oxide/graphene on reducing fire hazards of poly(butylene terephthalate). *J. Hazard. Mater*. 2014, 278, 391-400.

(15) Rakotomalala, M.; Wagner, S.; Döring, M. Recent developments in halogen free flame retardants for epoxy resins for electrical and electronic applications. *Materials.* **2010***, 3,* 4300-4327.

(16) Cui, W.; Du, F. P.; Zhao, J. C.; Zhang, W.; Yang, Y. K.; Xie, X. L.; Mai, Y. W. Improving thermal conductivity while retaining high electrical resistivity of epoxy composites by incorporating silica-coated multi-walled carbon nanotubes. *Carbon*. **2011**, **49**, 495-500.

(17) Chen, C.; Tang, Y. J.; Ye, Y. S.; Xue, Z. G.; Xue, Y.; Xie, X. L.; Mai, Y. W. High-performance epoxy/silica coated silver nanowire composites as underfill material for electronic packaging. *Compos. Sci. Technol.* **2014***, 105,* 80-85.

(18) Jiang, J. W. Graphene versus MoS2: A short review. *Front Phys-BEIJING.* **2015**, *10*, 1-16.

(19) Wang, D.; Zhou, K. Q.; Yang, W.; Xing, W. Y.; Hu, Y.; Gong, X. L. Surface modification of graphene with layered molybdenum disulfide and their synergistic reinforcement on reducing fire hazards of epoxy resins. *Ind. Eng. Chem. Res.* **2013**, *52*, 17882-17890.

(20) Lattimer, R. P.; Kroenke, W. J. The functional role of molybdenum trioxide as a smoke retarder additive in rigid poly(vinyl chloride). *J. Appl. Polym. Sci.* **1981**, *26*, 1191-1210.

(21) Stoeva, S.; Karaivanova, M.; Benev, D. Poly(vinyl chloride) composition. II. Study of the flammability and smoke-evolution of unplasticized poly(vinyl chloride) and fire-retardant additives. *J. Appl. Polym. Sci.* **1992**, *46*, 119-127.

(22) Tang, L. C.; Wan, Y. J.; Yan, D.; Pei, Y. B.; Zhao, L.; Li, Y. B.; Wu, L. B.; Jiang, J. X.; Lai, G. Q. The effect of graphene dispersion on the mechanical properties of graphene/epoxy composites. *Carbon*. **2013**, *60*, 16-27.

(23) Daniloska, V.; Keddie, J. L.; Asua, José M.; Tomovsk, R. MoS2 nanoplatelet fillers for enhancement of the properties of waterborne pressure-sensitive adhesives. *ACS Appl. Mater. Interfaces*. **2014**, *6,* 22640-22648.

(24) Kuilla, T.; Bhadra, S.; Yao, D. H.; Kim, N. H.; Bose, S.; Lee, J. H. Recent advances in graphene based polymer composites. *Prog. Polym. Sci.* **2010***, 35,* 1350-1375.

(25) Monti, M.; Rallini, M.; Puglia, D.; Peponi, L.; Torre, L.; Kenny, J. M. Morphology and electrical properties of graphene-epoxy nanocomposites obtained by different solvent assisted processing methods. *Compos. Part A-Appl. S.* **2013**, *46*, 166-172.

(26) Vadukumpully, S.; Paul, J.; Mahanta, N.; Valiyaveettil, S. Flexible conductive graphene/poly(vinyl chloride) composite thin films with high mechanical strength and thermal stability. *Carbon*. **2011**, *49*, 198-205.

(27) Lee, C.; Yan, H.; Brus, L. E.; Heinz, T. F.; Hone, J.; Ryu, S. Anomalous lattice vibrations of single- and few-layer MoS_2. *ACS Nano*. **2010**, *4*, 2695-2700.

(28) Li, H.; Yin, Z. Y.; He, Q. Y.; Li, H; Huang, X.; Lu, G.; Fam, D. W. H.; Tok, A. L. Y.; Zhang, Q.; Zhang, H. Fabrication of single- and multilayer MoS2 film-based field-effect transistors for sensing NO at room temperature. *Small.* **2012**, *8*, 63-67.

(29) Zhou, K. G.; Mao, N. N.; Wang, H. X.; Peng, Y.; Zhang, H. L. A mixed-solvent strategy for efficient exfoliation of inorganic graphene analogues. *Angew. Chem., Int. Ed.* **2011**, *50,* 10839-10842.

(30) Kim, S. K.; Wie, J. J.; Mahmood, Q. Anomalous nanoinclusion effects of 2D MoS2 and WS2 nanosheets on the mechanical stiffness of polymer nanocomposites. *Nanoscale*. **2014**, *6,* 7430- 7435.

(31) Lee, Y. H.; Zhang, X. Q.; Zhang, W. J.; Chang, M. T.; Lin, C. T.; Chang, K. D.; Yu, Y. C.; Wang. J. T. W.; Chang, C. S.; Li, L. J.; Lin, T. W. Synthesis of large-area MoS2 atomic layers with chemical vapor deposition. *Adv. Mater.*, **2012**, *24,* 2320-2325.

(32) Quinn, M. D. J.; Ho, N. H.; Notley, S. M. Aqueous dispersions of exfoliated molybdenum disulfide for use in visible-light photocatalysis. *ACS Appl. Mater. Interfaces*. **2013**, *5,* 12751-12756.

(33) Liu, Y. Y.; Tang, J.; Chen, X. Q.; Xin, J. H. Decoration of carbon nanotubes with chitosan. *Carbon.* **2005***, 43,* 3178-3180.

(34) Ilium, L. Chitosan and its use as a pharmaceutical excipient. *Pharm Res-Dordr*. **1998**, *15,* 1326-1331.

(35) Tang, Z. H.; Wei, Q. Y.; Guo, B. A generic solvent exchange method to disperse MoS2 in organic solvents to ease the solution process. *Chem. Commun.* **2014***, 50,* 3934-3937.

(36) Illy, N.; Benyahya, S.; Durand, N.; Auvergne, R.; Caillol, S.; David, G.; Boutevin, B. The influence of formulation and processing parameters on the

thermal properties of a chitosan–epoxy prepolymer system. *Polym. Int.* **2014**, *63,* 420-426.

(37) Balendhran, S.; Ou, J. Z.; Bhaskaran, M; Sriram, S.; Ippolito, S.; Vasic, Z.; Kats, E.; Bhargava, S.; Zhuiykov, S.; Kalantar-zadeh, K. Atomically thin layers of MoS2via a two step thermal evaporation–exfoliation method. *Nanoscale*. **2012**, *4*, 461-466.

(38) Najmaei, S.; Ajayan, P. M.; Lou, J. Quantitative analysis of the temperature dependency in Raman active vibrational modes of molybdenum disulfide atomic layer. *Nanoscale*. **2013**, *5,* 9758-9763.

(39) Wang, K. P.; Wang, J.; Fan, J. T.; Lotya, M; O'Neill, A; Fox, D.; Feng, Y. Y.; Zhang, X. Y.; Jiang, B. X.; Zhao, Q. Z.; Zhang, H. Z.; Coleman, J. N.; Zhang ,L.; Blau, W. J. Ultrafast saturable absorption of two-dimensional MoS2 nanosheets. *ACS Nano.* **2013***, 7,* 9260-9267.

(40) Liu, J. Q.; Zeng, Z. Y.; Cao, X. H.; Lu, G.; Wang, L. H.; Fan, Q. L.; Huang, W.; Zhang, H. Preparation of MoS2-polyvinylpyrrolidone nanocomposites for flexible Nonvolatile rewritable memory devices with reduced graphene oxide electrodes. *Small.* **2012***, 8,* 3517-3522.

(41) Splendiani, A.; Sun, L.; Zhang, Y.; Li, T.; Kim, J.; Chim, C. Y.; Galli, G.; Wang, F. Emerging photoluminescence in monolayer MoS2. *Nano Lett.* **2010**, *10,* 1271-1275.

(42) Tao, L. L.; Long, H.; Zhou, B.; Yu, S. F.; Lau, S. P.; Chai, Y.; Fung, K. H.; Tsang, Y. H.; Yao, J. Q.; Xu, D. G. Preparation and characterization of few-layer

MoS2 nanosheets and their good nonlinear optical responses in the PMMA matrix. *Nanoscale*. **2014**, *6,* 9713-9719.

(43) Bang, G. S.; Nam , K. W.; Kim, J. Y.; Shin, J.; Choi, J. W.; Choi, S. Y. Effective liquid-phase exfoliation and sodium ion battery application of MoS2 nanosheets. *ACS Appl. Mater. Interfaces*. **2014**, *6,* 7084-7089.

(44) Paulino, A. T.; Simionato, J. I.; Garcia, J. C.; Nozaki, J. Characterization of chitosan and chitin produced from silkworm crysalides. *Carbohyd. Polym.* **2006***, 64, 98-103.*

(45) Zhou, K. Q.; Jiang, S. H.; Bao, C. L.; Song, L.; Wang, B. B.; Tang, G.; Hu, Y.; Gui, Z. Preparation of poly(vinyl alcohol) nanocomposites with molybdenum disulfide (MoS2): structural characteristics and markedly enhanced properties. *RSC Adv.* **2012**, *2***,** 11695-11703.

(46) Alamri, H.; Low, I. M. Effect of water absorption on the mechanical properties of nano-filler reinforced epoxy nanocomposites. *Mater. Design*. **2012**, *42,* 214-222.

(47) Zhou, Y, X.; Jeelani, M. I.; Jeelani, S. Development of photo micrograph method to characterize dispersion of CNT in epoxy. *Mat. Sci. Eng. A-Struct.* **2009**, *506,* 39- 44.

(48) Chen, X. L.; Hu, Y.; Jiao, C. M.; Song, L. Preparation and thermal properties of a novel flame-retardant coating. *Polym. Degrad. Stabil.* **2007**, *92,*1141-1150.

(49) Tsai, K. C.; Park, H. C.; Jung, J. H.; Yoon, O. J.; Park, J. S.; Yoon, M. Y.; Lee, N. E. Orientation effect on cone calorimeter test results to assess fire hazard of

materials. *J. Hazard. Mater.* **2009**, *172,* 763-772.

(50) Wang, X.; Zhou, S.; Xing, W. Y.; Yu, B.; Feng, X. M.; Song, L.; Hu, Y. Self-assembly of Ni–Fe layered double hydroxide/graphene hybrids for reducing fire hazard in epoxy composites. *J. Mater. Chem. A*. **2013**, *1,* 4383-4390.

(51) Tai, Q. L.; Hu, Y.; Yuen, R. K. K.; Song, L.; Lu, H. L. Synthesis, structure-property relationships of polyphosphoramides with high char residues. *J. Mater. Chem.* **2011**, *21,* 6621-6627.

(52) Jiang, J.; Cheng, Y.; Liu, Y.; Wang, Q.; He Y., Wang, B. Intergrowth charring for flame-retardant glass fabric-reinforced epoxy resin composites. *J. Mater. Chem.* A. **2015**, *3*, 4284 -4290.

(53) Liu, Y.; Li, J.; Wang, Q. The investigation of melamine polyphosphate flame retardant polyamide-6/inorganic siliciferous filler with different geometrical form. *J. Appl. Polym. Sci.* **2009**, *113*, 2046 -2051.

Table 1. The data of cone calorimeter tests of neat EP and its composites.

Sample	**TTI (s)**	**PHRR (kW/m^2)**	**THR (MJ/m^2)**	**FGI ($kW/(m^2\cdot s)$)**
EP	65	1592	39.7	17.3
0.5wt%CS-MoS_2/EP	71	1243	35.9	12.4
1 wt%CS-MoS_2/EP	74	1107	28.6	12.2
2 wt%CS-MoS_2/EP	75	902	33.9	8.4
2 wt%MoS_2/EP	72	1178	40.1	11.8

Figure Captions

Scheme 1 Schematic illustration for exfoliating MoS_2 nanosheets by ultrasonication in chitosan aqueous solution and dispersing CS-MoS_2 nanosheets in tetrahydrofuran by the solvent exchange method.

Fig. 1 TEM images of bulk MoS_2 (a) and the ultrathin CS-MoS_2 nanosheets (b); AFM images (c) and thickness profiles (d) of CS-MoS_2 nanosheets.

Fig. 2 (a) Raman spectrum of bulk MoS_2 and CS-MoS_2 nanosheets obtained after ultrasonic exfoliation; Insets of (a) show the schematic of the E^1_{2g} and A_{1g} vibration modes. (b) UV/Vis spectra of CS-MoS_2 and pure chitosan in acetum.

Fig. 3 FT-IR spectra and TG curves of CS, MoS_2 and CS-MoS_2.

Fig. 4 SEM images of the fracture surface of neat EP (a), 0.5 wt% CS-MoS_2/EP (b), 2 wt% CS-MoS_2/EP (c, e) and 2 wt% bulk MoS_2/EP (d, f) nanocomposites.

Fig. 5 TEM observation of the ultrathin section of 2 wt% bulk MoS_2/EP (a) and CS-MoS_2/EP (b) nanocomposites.

Fig. 6 TG and DTG curves of neat EP and its nanocomposites in air atmosphere.

Fig. 7 HRR curves of neat EP and its nanocomposites derived from MCC.

Fig. 8 HRR curves of neat EP and its nanocomposites derived from cone calorimeter.

Fig. 9 Absorbance of toxic volatiles of neat EP, 2 wt% CS-MoS_2/EP and MoS_2/EP nanocomposite: (a) total pyrolysis products (Gram-Schmidt), (b) aromatic compounds, (c) CO and (d) hydrocarbons.

Fig. 10 SEM images of external (a) and internal (b) char residues.

Fig. 11 Raman spectra of internal char residues of neat EP and its nanocomposites.

Fig. 12 Dispersion sketch of CS-MoS_2 and bulk MoS_2 nanosheets in EP matrix.

Fig. 13 Visualization diagram of the flaming CS-MoS_2/EP nanocomposites.

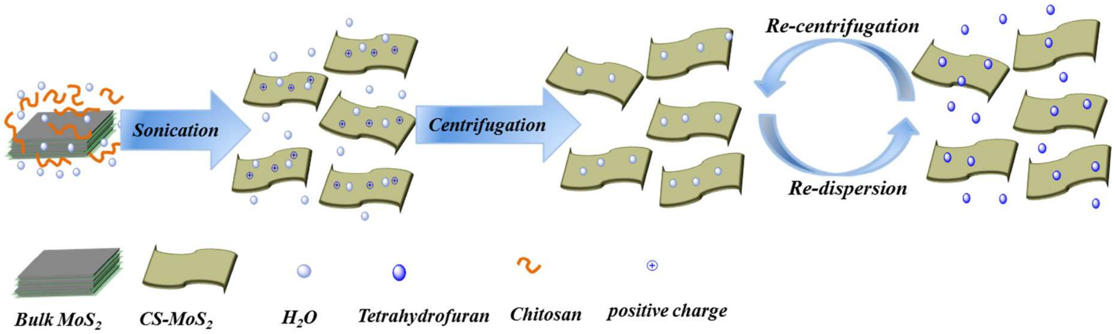

Scheme 1 Schematic illustration for exfoliating MoS_2 nanosheets by ultrasonication in chitosan aqueous solution and re-dispersing CS-MoS_2 nanosheets in tetrahydrofuran by the solvent exchange method.

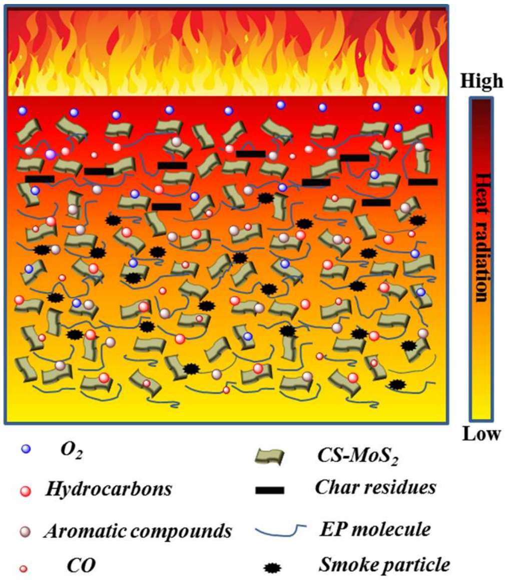

Scheme 2 Schematic illustration of nano-barrier effects of the flaming CS-MoS_2/EP nanocomposites.

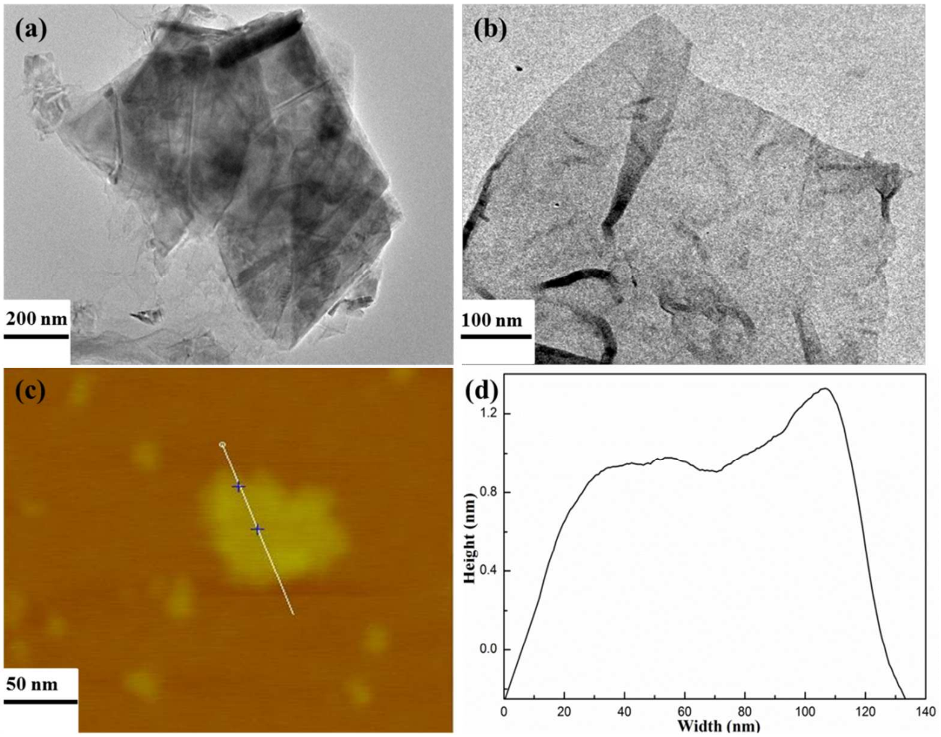

Fig. 1 TEM images of bulk MoS_2 (a) and the ultrathin CS-MoS_2 nanosheets (b); AFM images (c) and thickness profiles (d) of CS-MoS_2 nanosheets.

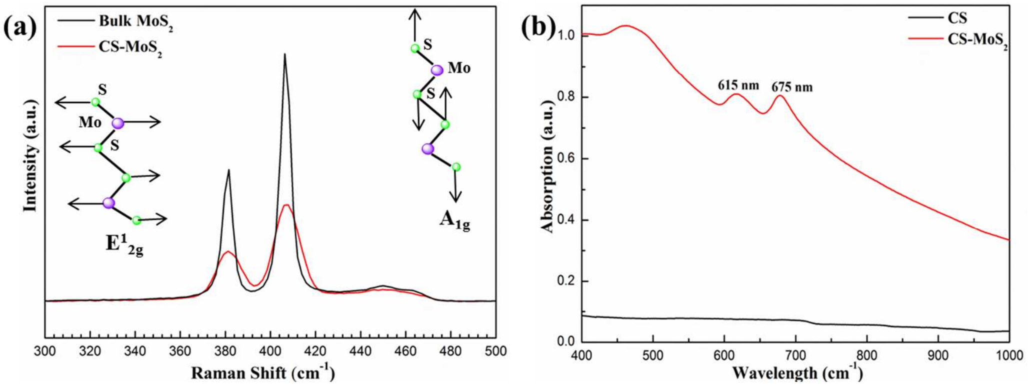

Fig. 2 (a) Raman spectrum of bulk MoS_2 and CS-MoS_2 nanosheets obtained after ultrasonic exfoliation; Insets of (a) show the schematic of the E^1_{2g} and A_{1g} vibration modes. (b) UV/Vis spectra of CS-MoS_2 and pure chitosan in acetum.

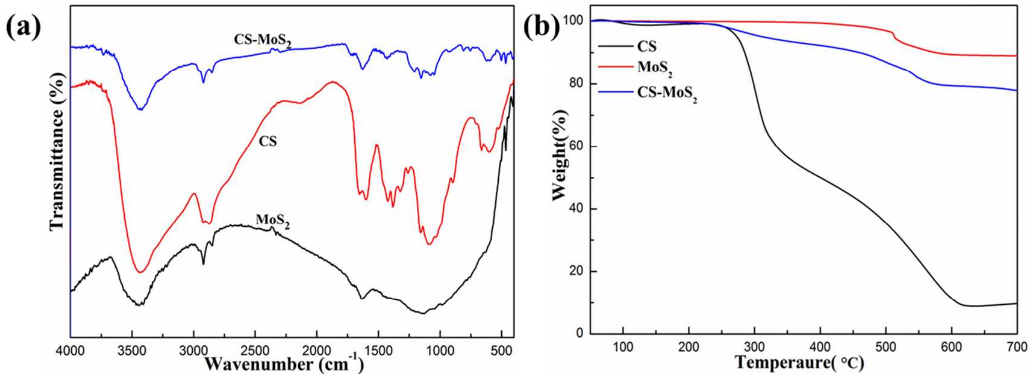

Fig. 3 FT-IR spectra and TG curves of CS, MoS_2 and CS-MoS_2.

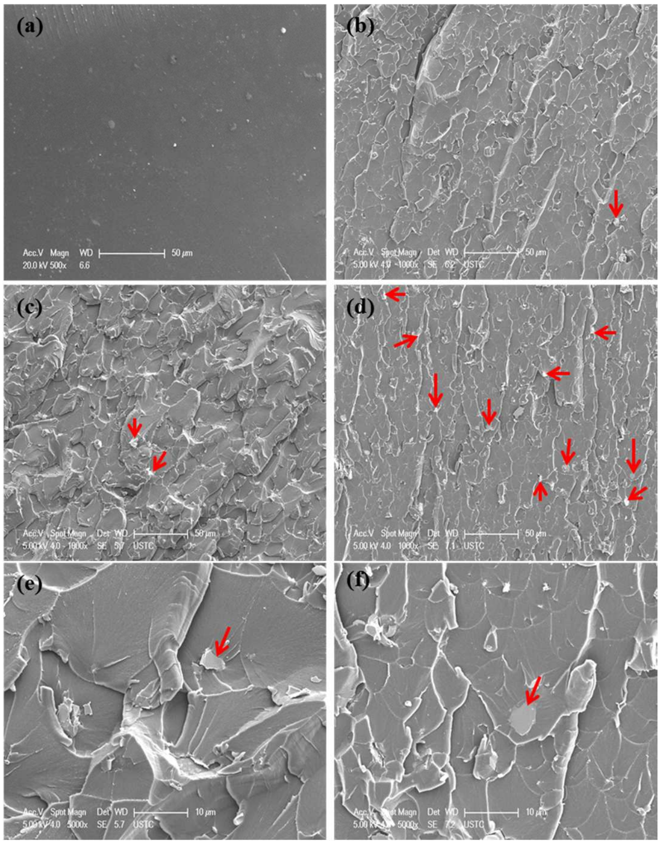

Fig. 4 SEM images of the fracture surface of neat EP (a), 0.5 wt% CS-MoS_2/EP (b), 2 wt% CS-MoS_2/EP (c, e) and 2 wt% bulk MoS_2/EP (d, f) nanocomposites (Red arrow points MoS_2 aggregates).

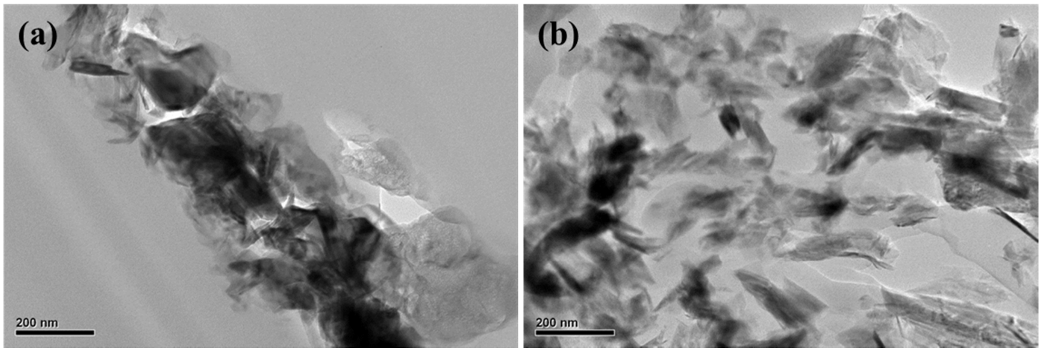

Fig. 5 TEM observation of the ultrathin section of 2 wt% bulk MoS_2/EP (a) and CS-MoS_2/EP (b) nanocomposites.

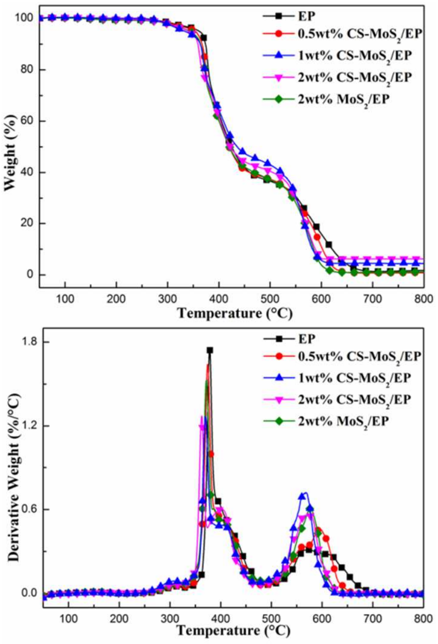

Fig. 6 TG and DTG curves of neat EP and its nanocomposites in air atmosphere.

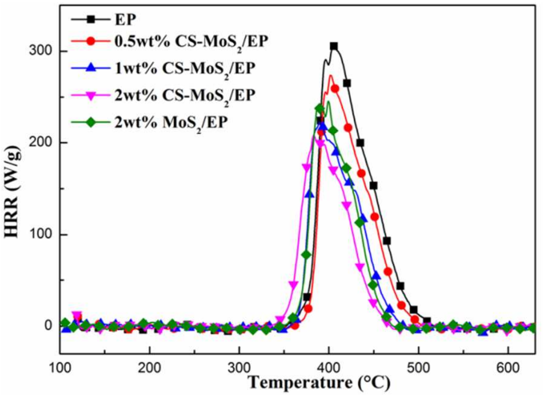

Fig. 7 HRR curves of neat EP and its nanocomposites derived from MCC.

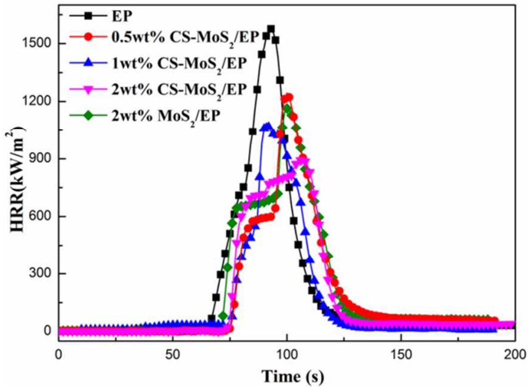

Fig. 8 HRR curves of neat EP and its nanocomposites derived from cone calorimeter.

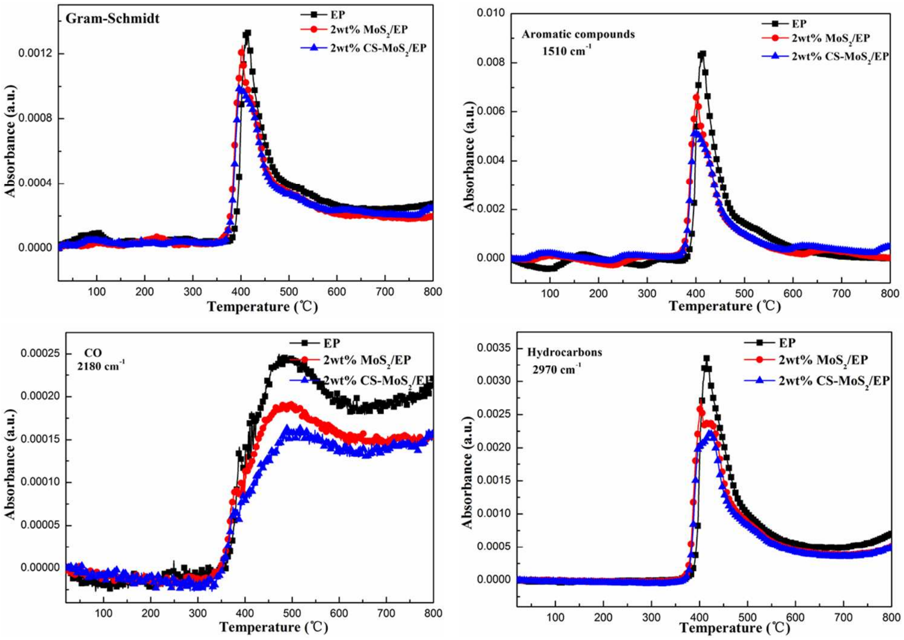

Fig. 9 Absorbance of toxic volatiles of neat EP, 2 wt% CS-MoS_2/EP and MoS_2/EP nanocomposite: (a) total pyrolysis products (Gram-Schmidt), (b) aromatic compounds, (c) CO and (d) hydrocarbons.

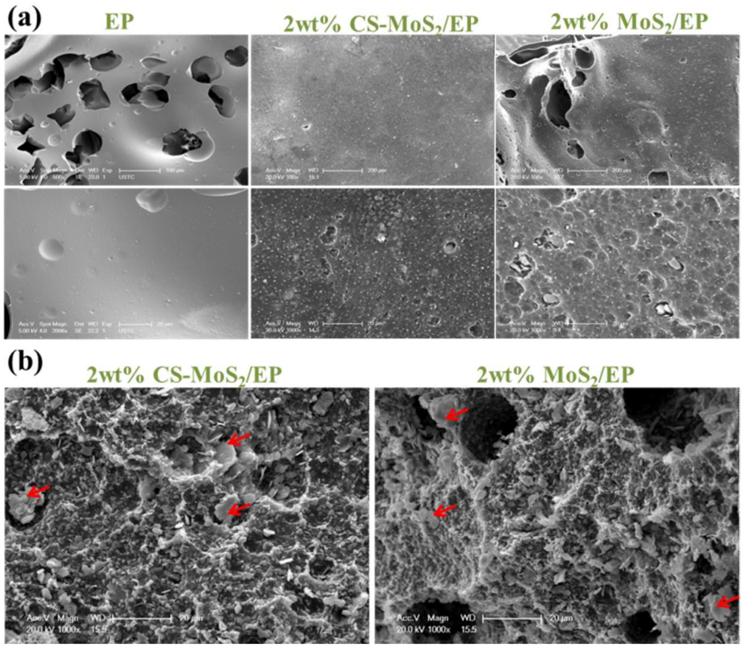

Fig. 10 SEM images of external (a) and internal (b) char residues.

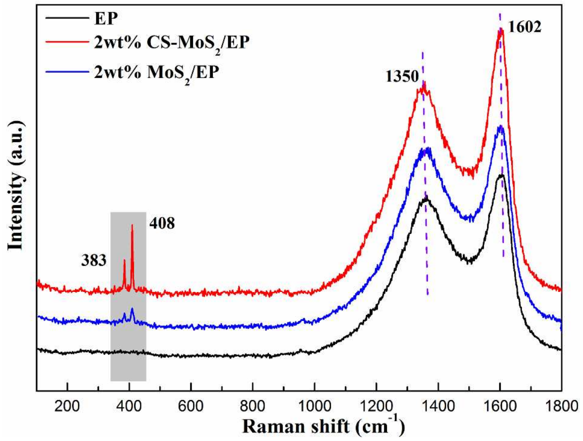

Fig. 11 Raman spectra of internal char residues of neat EP and its nanocomposites.

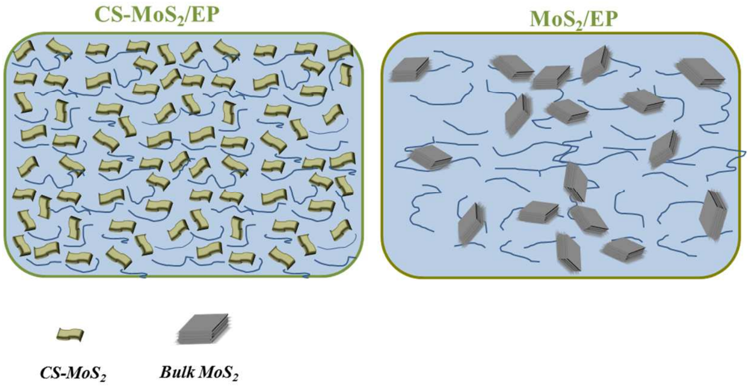

Fig. 12 Dispersion sketch of CS-MoS_2 and bulk MoS_2 nanosheets in EP matrix.